ResearchGate

See discussions, stats, and author profiles for this publication at: https://www.researchgate.net/publication/46254491

Reversible Resistive Switching and Multilevel Recording in La0.7Sr0.3MnO3 Thin Films for Low Cost Nonvolatile Memories

ARTICLE *in* NANO LETTERS · OCTOBER 2010

Impact Factor: 13.59 · DOI: 10.1021/nl1008162 · Source: PubMed

CITATIONS
59

READS
37

6 AUTHORS, INCLUDING:

Sergio Valencia
Helmholtz-Zentrum Berlin
88 PUBLICATIONS **1,576** CITATIONS
SEE PROFILE

F. Kronast
Helmholtz-Zentrum Berlin
80 PUBLICATIONS **1,002** CITATIONS
SEE PROFILE

Xavier Obradors
Materials Science Institute of Barcelona
650 PUBLICATIONS **8,472** CITATIONS
SEE PROFILE

Carmen Ocal
Materials Science Institute of Barcelona
115 PUBLICATIONS **2,411** CITATIONS
SEE PROFILE

Available from: Sergio Valencia
Retrieved on: 30 January 2016

NANO LETTERS

pubs.acs.org/NanoLett

Reversible Resistive Switching and Multilevel Recording in $La_{0.7}Sr_{0.3}MnO_3$ Thin Films for Low Cost Nonvolatile Memories

César Moreno,[†] Carmen Munuera,[†] Sergio Valencia,[‡] Florian Kronast,[‡] Xavier Obradors,[†] and Carmen Ocal*,[†]

[†]Institut de Ciència de Materials de Barcelona, CSIC, Campus de la UAB, 08193-Bellaterra, Spain, and [‡]Helmholtz-Zentrum-Berlin, Albert-Einstein-Strasse 15, D-12489, Berlin, Germany

ABSTRACT On the basis of a scanning probe microscopy strategy, we propose a combined methodology capable to program nonvolatile multilevel data and read them out in a noninvasive manner. In the absence of the common two-electrode cell geometry, this nanoscale approach permits, in addition, investigating the relevance of inherent film properties. We demonstrate the feasibility of modifying the local electronic response of $La_{0.7}Sr_{0.3}MnO_3$ to obtain nanostructures with switchable resistance embedded in low cost oxide thin films, which constitutes a promising approach for fabricating high density nonvolatile memories.

KEYWORDS Resistive switching, Kelvin probe microscopy, RRAM, transition metal oxides

Resistive switching memory devices (ReRAM) are based on one of the most promising nonvolatile data storage concepts to replace conventional devices like EEPROM or Flash. The switching between two distinct resistive states is electrically controlled, in current and/or voltage depending upon the nature of the material integrated in the memory cell. In particular, reversible resistive switching in correlated oxides is widely investigated at present because of its strong potential for fabricating multiple-bits-per-cell resistive memories, which would considerably increase the storage density capabilities of any conceivable device.

Basic ReRAM research is by far not new. It begun almost 40 years ago with works on oxide insulators[1] and amorphous materials.[2] Among the different materials (semiconductors,[3−5] ferroelectric,[6,7] ferromagnetic,[8] multiferroic,[9] and chalcogenoide[2]) for realizing a new solid-state nonvolatile memory technology,[10] transition metal oxides are pursued with increasing interest to provide devices with high areal densities, fast random access, virtually unlimited usage, and low power consumption.[11] Several types of oxides, such as $SrZrO_3$:Cr,[12] $SrTiO_3$:Cr,[13] CuO,[14] NiO,[15] TiO_2,[16,17] ZnO:Mn,[18] $Pr_{0.7}Ca_{0.3}MnO_3$,[19,20] and $La_{1-x}Sr_xMnO_3$[21,22] have been found to display electrically switchable resistivity in two-terminal geometry junctions (metal−insulator−metal, MIM). Multiple microscopic mechanisms have been proposed based either on redox processes involving cation or anion migration,[23,24] on the formation/rupture of conducting nanoscale filaments,[19,25−28] oxygen diffusion,[29] Mott metal−insulator transitions,[30,31] variable Schottky barriers,[32] or charge trapping at interfacial sites.[33] Very often, only macroscopic analyses are reported strongly limiting a detailed microscopic understanding. However, in the past few years, local scanning probe techniques have been incorporated as interesting tools for investigating resistive switching at the nanoscale.[28,34−38]

Here, we report on novel reversible transitions from low resistive (LR) to high resistivity (HR) states in well-characterized thin films of the robust metallic ferromagnet $La_{0.7}Sr_{0.3}MnO_3$ (LSMO) grown by chemical solution deposition (CSD)[39−41] on insulating $SrTiO_3$ (100) substrates. CSD has recently emerged as a very competitive technique for obtaining epitaxial films of high quality with controlled nanostructure. Sol gel science is now a well established discipline which has reached a wide use for the production of materials with high performance such as coated conductors, nanoparticles, bulk ceramics, hybrid materials, mesoporous solids, coatings, etc.[42−44] The main advantage of this methodology is that low capital investment and supply costs are envisaged, thus becoming a competitive alternative to vapor deposition techniques requiring the use of vacuum systems.

With the aim of elucidating the role of inherent LSMO thin film properties, we intentionally avoid the standard two-terminal MIM geometry. The transitions are induced at the nanoscale under the application of a bias voltage by means of the conducting tip of a scanning force microscope. In our setup, the sample was always grounded and the voltage was applied to the tip (first electrode). Provided the insulating character of the substrates, direct electric contact to ground was established through a metallic clamp (counter electrode) firmly attached to the surface film at the sample border (millimeters apart from the tip−surface contact). In such a

* To whom correspondence should be addressed, cocal@icmab.es.
Received for review: 03/7/2010
Published on Web: 09/13/2010

© 2010 American Chemical Society

DOI: 10.1021/nl1008162 | *Nano Lett.* **2010,** *10,* 3828–3835

way, we rule out specific interfacial phenomena (e.g., metal diffusion) or electrode interconnections (e.g., filamentary formation) which have been suggested as responsible for resistive switching. The mechanisms at the origin of the modifications induced in our $La_{0.7}Sr_{0.3}MnO_3$ thin films are investigated in the complete set and reset switching (writing and erasing) process. In particular, local conductance and contact potential difference (CPD) have been analyzed under low humidity conditions (<2 % RH) by combining conductive scanning force microscopy (C-SFM) and Kelvin probe microscopy (KPM). This approach, which is based on the use of a single tip for writing, reading, and erasing, has important implications for the development of multifunctional memory devices.

The transition can be induced through the full thickness of the films such that, using specific writing geometries, conducting regions can be topologically isolated. Depending on the magnitude of the applied tip voltage, different final states can be achieved. KPM is revealed as a valuable reading tool for the multilevel adscription by means of work function measurements. Local compositional and valence changes associated to the written and erased states have been revealed by photoemission electron microscopy (PEEM) at the Mn $L_{3,2}$-, La $M_{5,4}$-, and O K-edges.

Starting from a conducting state, our goal is using a low energy consumption operation onset mechanism to reach a multilevel system with switchable resistance forming arrays of nanostructures embedded in low cost oxide thin films. This capability can be easily envisaged as a suitable approach toward active electronic elements, in particular for the fabrication of high-density data storage applications.

Thin films of the robust metallic ferromagnet $La_{0.7}Sr_{0.3}MnO_3$ are especially appealing because the possibility to have in the same material electroresistance effects and magnetorresistance properties. However, bistable switching in this material has only been observed in some metal/LSMO junctions as Au/LSMO[21] and Ag/LSMO,[45] where the corresponding observations were attributed to particular interfacial characteristics such as roughness, spatial inhomogeneities, or electrode metal diffusion into the oxide film. The later being a common interpretation in other MIM systems classified within the so-called electrochemical metallization mechanisms (ECM).[46] Unfortunately, the MIM junction geometry usually prevents access to analyze the buried metal/LSMO interface. In the present study, the direct observation of the locally induced modifications permits investigating the role of inherent properties of the LSMO films, an important step forward to the control of electroresistance systems.

To demonstrate that the switching procedure does not depend on particular thin film details, results for LSMO ultrathin films prepared by the same CSD method but different thicknesses (8, 10, and 24 nm) and diverse surface morphologies are presented. We first illustrate a complete writing, reading, and erasing process performed on a 24 nm thick LSMO film (sample 1). The sample surface (Figure 1a) exhibits a certain concentration of outcropped La−Sr oxide (LSO) nanodots (∼50−80 nm high), which are the controlled result of a La excess in the chemical solution and, as it has been already reported,[40] do not influence the physical properties of the surrounding metallic LSMO film. As expected, they exhibit an insulating character, as seen in the current map taken at a tip voltage $V_{tip} = -2$ V (Figure 1b) and therefore constitute an excellent in situ reference for topographic and conducting experiments. Because no changes in the electrical properties of the film were observed at this voltage value after repeated sweeping, it will be used as the reading voltage ($V_{rd} = -2$ V) throughout the following experiments.

Electrical switching between LR (ON) and HR (OFF) was accomplished by a systematic approach performed under low humidity conditions in the repulsive contact regime (Supporting Information, Methods), then the existence of any water neck between tip and sample can be ruled out. The concentric squares in Figure 1a correspond to the writing/erasing (inner square) and reading (outer square) regions, respectively. The reading step in Figure 1c shows that after scanning at a voltage of $V_{wr} = +4$ V the writing region presents a nonconducting character; i.e., it has been completely transformed to a HR state. At this point, the LSO nanodots are no longer distinguished from the rest of the film. Panels d−f of Figure 1 illustrate three steps (−3, −4, and −5 V) of an erasing process. The electrical transition is completely reversed for $V_{er} = -5$ V. Interestingly, a close inspection of Figure 1d allows observing that the conducting character does reverse at lower voltages in the near surroundings of the LSO nanoislands than in the rest of the LSMO film. This observation can be attributed to locally slightly different film thickness, to the effect of the local strain induced in the LSMO film at the boundaries with the LSO nanodots,[40] or to the existence of charge traps associated to point defects or a local redistribution of atomic species.

Figure 2a shows a typical $I-V$ characteristic or bipolar switching curve conducted by application of a voltage cycle (±10 V) at a fixed tip location on the virgin (preswitched) surface of a 10 nm thick LSMO thin film (sample 2). The clearly asymmetric curve indicates that diverse microscopic processes govern charge transport under each polarity, and thus, the different branches of voltage sweep ($-10 \rightarrow 0 \rightarrow +10 \rightarrow 0 \rightarrow -10$) can be separately analyzed. At negative V_{tip} values, the current initially follows a conducting (LR) Ohmic excursion, with a slope that markedly decreases at small voltages (-0.5 V $< V_{tip} < +0.5$ V) reflecting a nonnegligible tip−film surface contact resistance. At positive voltages, the current increases linearly again until the current suddenly drops, at $V_{tip} = +5$ V. This critical voltage is considered as the set point, V_{SET}, for switching from LR to HR. In this particular case, the conductance ratio is $I_{ON}/I_{OFF} \approx 10^2$. As better seen in the clearly hysteretic semilogarithmic plot of Figure 2b, the current stays at very low values

© 2010 American Chemical Society

DOI: 10.1021/nl1008162 | Nano Lett. 2010, 10, 3828–3835

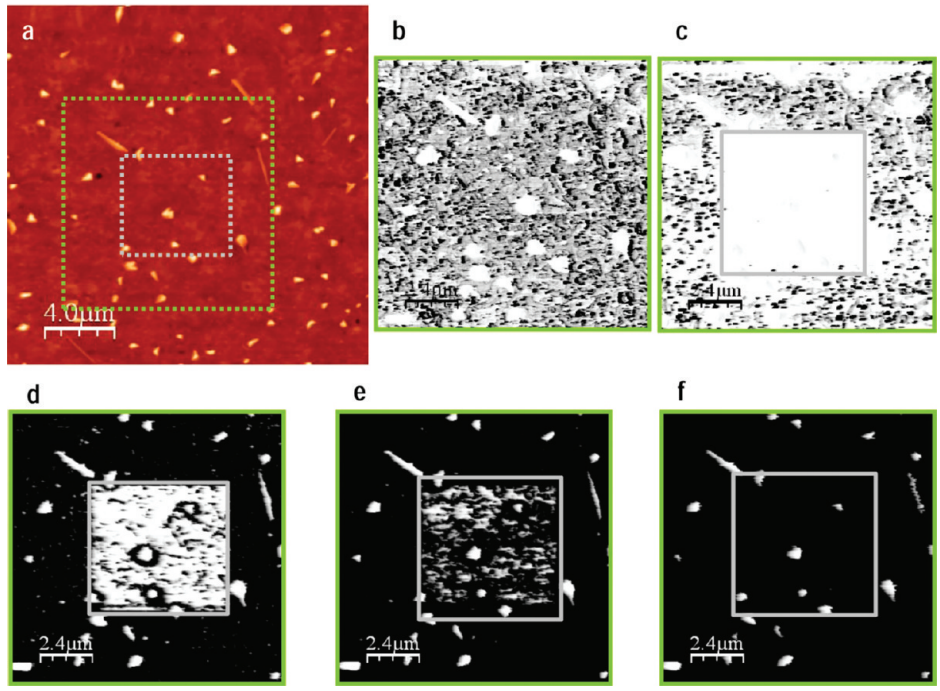

FIGURE 1. Resistance switching movie: writing, reading, and erasing the local conducting properties of LSMO. The reversible transition between low resistive (LR) and high resistive (HR) states is performed (writing and erasing at appropriates V_{tip}) and followed (reading at noninvasive V_{rd}) by conducting scanning force microscopy (C-SFM). (a) Topographic image (20 μm $\times$ 20 μm) of a 24 nm thick LSMO thin film (sample 1). A certain concentration of outcropped insulating (La−Sr oxide (LSO) nanodots (50−80 nm high) are used as in situ reference for topographic and conductivity measurements. Concentric squares on the image correspond to the writing/erasing (inner square) and reading (outer square) regions, respectively. (b, c) Reading current maps taken at $V_{rd} = -2$ V, before (virgin state) and after writing a HR state at $V_{wr} = +4$ V. The nonconducting character of the written region is reversed by changing the voltage polarity. (d, e, and f) Reading current maps during the erasing process performed in three steps, $V_{er} = -3$, -4, and -5 V. The conducting character of the initial LSMO is recovered. As seen, the electrical transition is completely reversible for $V_{er} = -5$ V. Note that because $V_{er} > V_{rd}$, more current is detected in (d), (e), and (f) than in (b) and (c). Color code goes from 0 to 100 nm in the topographic image and saturates at 100 nA in the current maps.

all the rest of the positive branch, i.e., until $V_{max} = +10$ V. The system remains at this HR state during the voltage back excursion. Under conditions of reverse bias, considerable electronic current is restored only after a sufficiently large opposite polarity, $V_{tip} \approx -8$ V. At this reset voltage, a sharp current injection drives the system to the initial conducting state, where it remains until completing the voltage cycle (−10 V). The robustness of the process was verified by endurance test consisting of consecutive bipolar switching curves conducted on the same location (Figure 2c). Though a change in the reset voltage accompanied by staircase behavior was eventually observed, the switching persisted. Moreover, the polarity of the set (LR−HR) and reset (HR−LR) voltages was in each case always the same, independently of the cycle direction.

In contrast to the otherwise expected linear *IV* relationship of the conducting state of the LSMO film, the conduction mechanisms operating after the LR−HR transition seem not evident and deserve some attention. In an attempt to elucidate about these mechanisms in different MIM systems presenting similar resistive switching characteristics, separate fits of the HR branches have been proposed.[47−50] In particular, the asymmetric Schottky-like behavior observed in our case ($+10 \rightarrow 0 \rightarrow V_{RESET}$) reminds those in which the closed state ($+10 \rightarrow 0$) has been correlated to transport dominated by a space-charge-limited (SCL) conduction due to a depletion of the film, while for negative bias ($0 \rightarrow V_{RESET}$) a large reverse-biased barrier of the electrode contact originates a Schottky controlled conduction. In this context, the top electrode−oxide interface nature is of great importance since varying the interface barrier height, for instance by introducing a thin insulating layer between metal electrode and LSMO film, the device properties can be controlled.[46,51] Far from the common two-terminal MIM geometry, our experimental design consists of a mobile electrode−LSMO interface (scanning tip-topmost film surface contact). However, even if some interfacial mechanisms can take place during scanning, we will demonstrate that the film can be electrically modified through its whole thickness, and these modifications persist in the absence of the mobile interface, pointing to the relevance of inherent properties of the LSMO films to the resistive switching.

The process described in Figure 1 can be conducted at different V_{wr} larger than V_{SET} such that the corresponding reset voltage V_{RESET} depends on the specific V_{wr} used (see Figure S2 in Supporting Information) and is found to be $V_{RESET} \sim -V_{wr}$. This result is already evidence of tunable multilevel recording in LSMO and will be discussed in depth below. In order to exploit the storage capabilities of the process and to know about its spatial extent in depth, we

© 2010 American Chemical Society

DOI: 10.1021/nl1008162 | *Nano Lett.* **2010,** *10,* 3828–3835

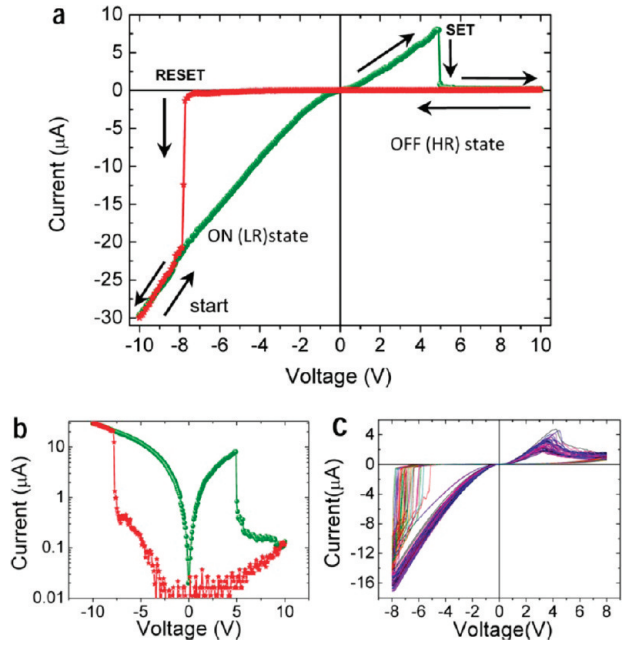

FIGURE 2. Local current−voltage characteristics and endurance test. (a) Hysteretic bipolar switching $I-V$ curves for a 10 nm thick LSMO thin film (sample 2). The duration of the cycle is $\tau = 76$ ms. Starting from a conducting (LR) state, the voltage ramp is applied to the tip from negative to positive values and back to complete the cycles as indicated by the arrows. SET (LR to HR) and RESET (HR to the initial LR) points are marked in what is the first $I-V$ cycle. LR and HR are identified as ON and OFF, indicating the pass or blockage of electronic current through the device. (b) Logarithmic scale plot of the $I-V$ in (a) showing the abrupt change in conductivity (large $I_{ON}/I_{OFF} > 100$) at the operation SET. (c) Endurance test (shown 100 out of 500 $I-V$ cycles). Though apparent, there is no reduction of the reset voltage but random deviations of a relatively constant value (see Figure S1 in Supporting Information) and, importantly, the system maintains its switching behavior.

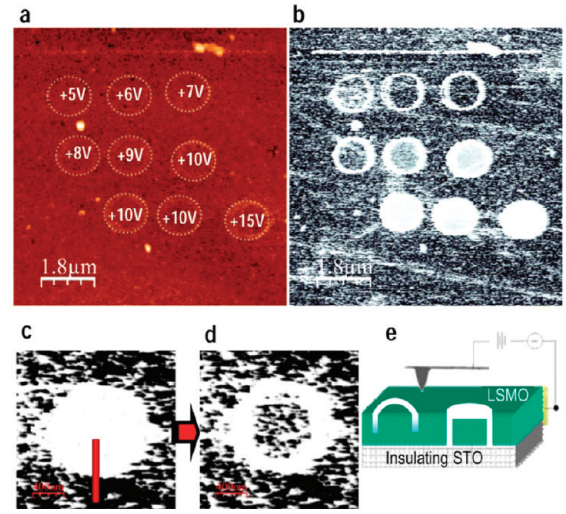

FIGURE 3. Full LSMO film thickness modification: voltage dependence of the writing process. (a and b) Simultaneously acquired topographic view (total scale 40 nm) and current map at $V_{rd} = -2$ V(total scale 100 nA) of a 10 nm thick LSMO thin film (sample 2). A lithographic C-SFM procedure has been used to write HR states with ring geometry at different V_{wr} from +5 to +15 V. From a given voltage threshold, nonmodified (LR) regions are electrically isolated, indicating the whole film thickness has been driven to the HR state. (c and d) Verification test: current images before and after a LR bridge connects the inner conducting region with the outer conducting LSMO film. The bridge LR state is induced by drawing a line crossing the HR ring (red line) with the tip at reversed polarity, $V_{er} = -10$ V. (e) Schematics of the process (cross section) and C-SFM setup. The tip is biased and the counter-tip electrode contact is established at the border of the sample. Wrong (nonsensitive) reading: no current can be detected on conducting LR regions which are enclosed by HR rings reaching the whole film thickness.

have employed a lithographic based strategy, similar to that employed in surface conductance measurements.[52,53] Figure 3 presents a series of modifications made with the conducting tip describing rings (dotted lines in Figure 3a) at different V_{wr}, on the same LSMO film (sample 2) with quite homogeneous morphology and conductance. As can be seen in the current map (Figure 3b), nonconducting rings were observed for $V_{tip} > +5$ V. Interestingly, for $V_{tip} > +10$ V negligible or no current was measured within the inner ring region. The lack of detectable current in that region, where no electrical change has been induced, points to a blockage of the electric current at the ring location and across the whole film thickness, which prevents electric flow between tip and the grounded electrode, placed at the sample border. This interpretation was confirmed by locally reversing the resistivity state along a tip trajectory crossing the ring as indicated by the solid line in Figure 3c. The electrical connection between the enclosed region and the rest of the metallic LSMO film is restored (Figure 3d). Such a simple experiment leads us to conclude that the film had been driven to the HR state throughout its whole thickness following the vertical component of the high electric field created at the tip apex, i.e., forming a nonconducting tube that completely blocks the current through the inner region, which becomes a topologically isolated volume (Figure 3e).

The above experiment demonstrates the local nature of the switching process, but as isolated conducting regions are not distinguished from insulating ones, a reading procedure different than C-SFM is clearly desired. In order to find an appropriate read-out tool, we performed combined C-SFM and KPM measurements in the very same region. An array of rings written at different voltages (Figure 4a) was lithographed in an 8 nm thick LSMO film (sample 3). Though a lower writing voltage ($V_{wr} = +2$ V) correlates with the smaller thickness of this film, the same observation described above for sample 2 can be seen in the C-SFM map (Figure 4b). Conversely, a notable piece of information is provided by the differences seen in the CPD image (Figure 4c), revealing KPM as a more sensitive tool to changes in the LSMO nature than C-SFM.

The film surface can be visualized as the top view of a series of HR hollow cylinders embedded in a thin LR matrix. A different potential barrier (electrostatic), i.e., a different surface potential, commonly identified with a different work function (Φ), exists depending on the local electronic properties.[55] When this barrier is higher (larger Φ), the surface CPD signal decreases. Knowing the CPD values for rings

© 2010 American Chemical Society

DOI: 10.1021/nl1008162 | Nano Lett. 2010, 10, 3828–3835

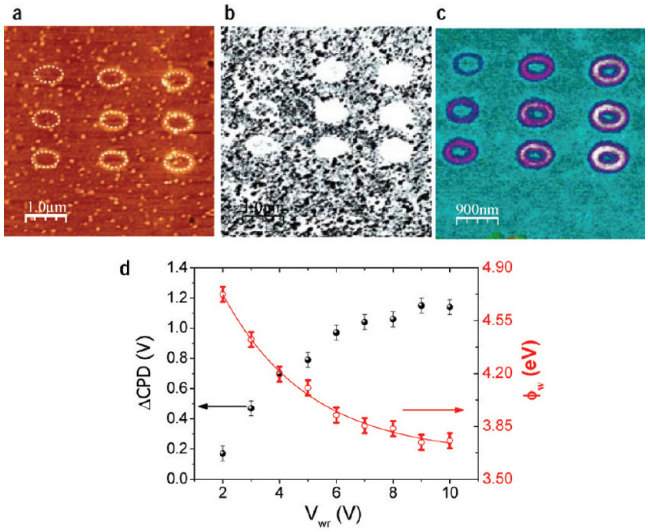

FIGURE 4. Combined C-SFM and KPM reading strategy and HR multilevel detection. C-SFM measurements are performed by placing the tip in direct contact with the sample whereas KPM are done in a noncontact dynamic mode (~10−30 nm apart). (a) Topographic view (total scale 4 nm) of a a 8 nm thick LSMO film (sample 3). The dotted lines indicate the written HR rings at different increasing voltages $V_{wr} = +2$ to $+10$ V, in steps of 1 V from top to bottom and left to right. (b) Simultaneous reading current map ($V_{rd} = -2.5$ V). Total current scale is 100 nA. (c) Contact potential difference (CPD) map as measured by KPM. A customized color scale has been used to highlight the discrete values of the surface potential and goes from cyan (0 V) to white (1.2 V). (d) Contact potential difference (left axis) relative to that of the LSMO virgin film (ΔCPD) as a function of V_{wr} and calculated local work function ($\Phi_w = \Phi_{LSMO} - \Delta CPD$) (right axis) for the different HR written states. $\Phi_{LSMO} = 4.9$ eV is taken from ref.[54] Importantly, KPM is sensitive to different HR states (correct reading and multilevel detection) not distinguishable in the C-SFM measurements.

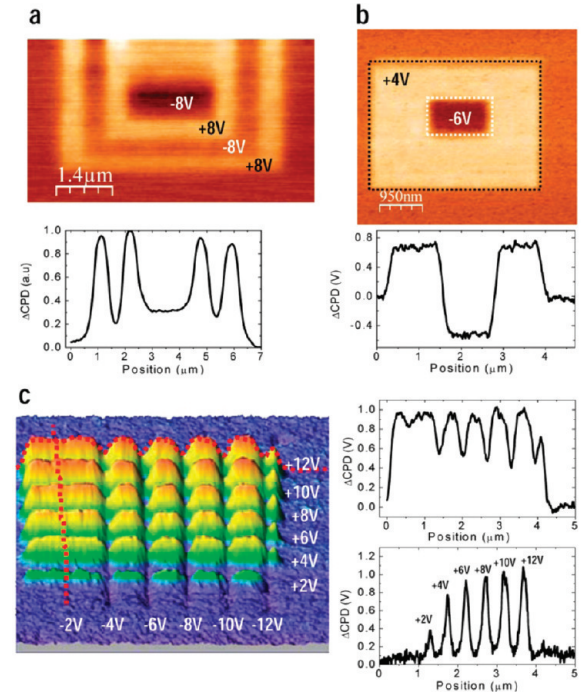

FIGURE 5. Reversible multilevel LR and HR data storage. (a) KPM image and corresponding ΔCPD line profile, of a sequence of writing and erasing processes performed one after the other over decreasing areas on a 10 nm thick LSMO film (sample 2) at opposite bias voltages ($V_{wr} = +8$ V and $V_{er} = -8$ V). (b) KPM image of a writing ($V_{wr} = +4$ V) and an erasing ($V_{er} = -6$ V) processes performed one after the other over decreasing areas on a 8 nm thick LSMO film (sample 3). The corresponding ΔCPD line profile shows the sensitivity of KPM to detect positive and negative changes in the local Φ_w, depending on the magnitude of the applied V_{wr} and V_{er}. (c) Three-dimensional view of a KPM image of a grid made of perpendicular crossing lines, C-SFM lithographed at different V_{wr} and V_{er} on sample 3 (left image). As can be seen in the profile along the crest at the top image ($V_{wr} = +12$ V) (upper right image), the lateral resolution of the CPD signal limits visualizing the reversed LR states. However, this preliminary example points to the capability of the procedure for bit storage in a multilevel device.

written at different voltages, the relative changes in work function (ΔΦ) can be obtained (Supporting Information, Methods). As seen in Figure 4d, ΔCPD > 0 (i.e., $\Phi_w < \Phi_{LSMO}$) and increases as a function of V_{wr} until it saturates. Using for the virgin surface the reported Φ_{LSMO},[54] we obtain $\Phi_w \sim 3.7$ eV for the lowest work function state ($\Delta\Phi_w \sim 1.15$ eV), independently of the LSMO film thickness. Charge carriers in lightly alkaline-earth-doped manganites as $La_{0.7}Sr_{0.3}MnO_3$ are holes, and then they can be regarded as p-type semiconductors. Thus, the simplest way to interpret the work function changes would be as due to a decrease of the carrier concentration (holes) under applied positive bias. Moreover, changes in atomic structure[27,56,57] and local composition, i.e., cation or anion distribution, cannot be neglected. With heteroepitaxial junctions, the Fermi level positions for $La_{1-x}Sr_xMnO_3$ have been reported to shift downward (increasing Φ_{LSMO}) with hole doping.[58] Within this context, our results would be consistent with a reduced x, lower than the initial $x = 0.3$. Note that the $La_{1-x}Sr_xMnO_3$ phase diagram predicts an insulating character for $x < 0.2$. Obviously, a similar behavior is expected for an increase in the amount of oxygen vacancies which would decrease the valence of the Mn ions. The consequent increase of e_g-electrons and change of carrier concentration would be responsible for a Fermi level shift.

Back to make use of the reversibility of the process, we show now the capability of KPM to read out and differentiate a variety of electronic states. Figure 5a shows the KPM image of a sequence of writing and erasing processes performed one after the other over decreasing areas (sample 2) at opposite bias voltages ($V_{er} = -V_{wr}$). In such a way, the central region has been modified four times (twice written and twice erased). The averaged CPD signal reflects the back and forth change in electrical nature of the modified film regions. Interestingly, if the negative voltage employed for erasing is larger in absolute value than for writing, work functions larger than that of the virgin state can be reached. This result is illustrated in Figure 5b. In short, the capability of the method goes beyond reversibility and serves to finely tune the work function by choosing the appropriate V_{wr} and V_{er}.

The switchable character of these nanoscale modifications is further evidenced in Figure 5c where six horizontal

© 2010 American Chemical Society

DOI: 10.1021/nl1008162 | Nano Lett. 2010, 10, 3828–3835

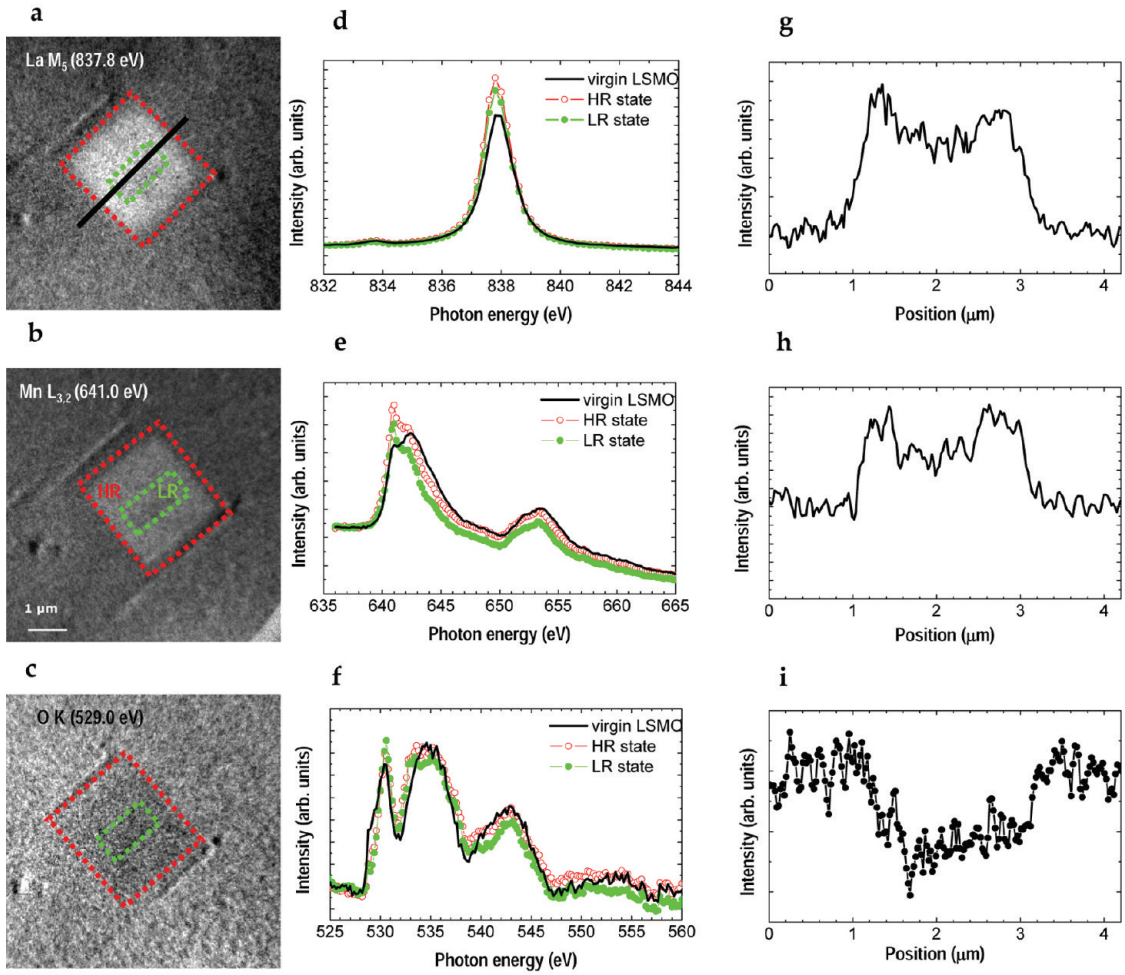

FIGURE 6. Atomic species distribution in switched HR and LR states. (a, b, and c) PEEM images obtained on a modified LSMO surface (sample 3) at selected energies (837.8, 641.0, and 529.0 eV) within the La M-, Mn L-, and O K-edges, respectively. The inside of a square written at $V_{wr} = +4$ V was reset using a $V_{er} = -6$ V. (d, e, and f) averaged spectra obtained within the virgin LSMO (black line), written HR state (red open dots) and erased LR state (green filled dots) regions at the La M-, Mn L-, and O K-edges, respectively. (g, h, and i) are the intensity profiles corresponding to the black continuous line in a, taken at the energies of the three absorption edges. These profiles cross the three regions of interest (virgin, HR, and LR) to show the clear change in atomic species.

lines have been lithographed at different V_{wr}, on the same surface. The vertical line profile crossing all the written lines is shown in the bottom plot of Figure 5c to obtain CPD versus V_{wr}. Lines perpendicularly lithographed at negative voltages complete a squared grid. At every cross of lines, a given high CPD state would be reset to a low CPD state. Though the erased states are slightly blurred due to overlap of adjacent high CPD signals, the horizontal profile taken along one line ($V_{wr} = +12$ V) illustrates the result (top plot of Figure 5c). Hills and valleys in CPD correspond to different surface potential states, respectively, and exemplify the capabilities of bit storage in a foreseen multilevel device (see Figure S3 in Supporting Information). Durability of the modifications were tested in time, temperature, and magnetic fields, and were found to persist after several months, upon annealing up to 400 K and show no detectable degradation under magnetic fields up to 3 T (see Figure S4 in Supporting Information).

Being aware of the importance in nature of the top electrode−oxide interface, here the outermost film surface in contact with the scanning tip or mobile electrode, we performed soft X-ray photoelectron emission microscopy (PEEM)[59] after a writing/erasing protocol similar to that described above. Taking into account the high surface sensitivity of this technique (~4 nm in depth), the ~8 nm thick LSMO film (sample 3) was used so that a representative film thickness is analyzed. A summary of the results is presented in Figure 6. An area including written (HR) and erased (LR) states over decreasing areas, was imaged at several photon energies across the La $M_{5,4}$-, Mn $L_{3,2}$-, and O K-edges. Unfortunately, the allowed experimental energy range did not permit access to obtain information about strontium. As can be seen in the PEEM images, Figure 6a−c, the modified surface areas exhibit very different compositional contrasts than the virgin LSMO.

© 2010 American Chemical Society

DOI: 10.1021/nl1008162 | *Nano Lett.* **2010,** *10,* 3828–3835

The central panels of Figure 6 present the averaged La (d), Mn (e), and O (f) spectra as a function of photon energy for the regions of interest, namely, virgin LSMO (continuous line), HR (open symbols), and LR (filled symbols). In all three spectra, the observable differences in intensity and/or shape between the virgin LSMO and the modified regions point to changes in atomic content and/or oxidation state. The La M_5-edge spectra (Figure 6d) taken at the three regions are identical with respect to shape and energy positions, as corresponds to a unique oxidation state for the lanthanum cations (La^{3+}) and permitting a direct correspondence between integrated intensities and the atomic contents within the analyzed depth. In this particular case, noticeable differences on the spectra relative maximum intensity highlight local changes of about 15% (HR) and 6% (LR) excess of La concentration. However, since the shape as well as the integrated intensity of the Mn L-edge strongly depend on the Mn oxidation state,[60,61] interpretation of the changes observed in the corresponding spectra (Figure 6e) are not so evident. On one hand, the virgin LSMO region depicts a Mn L-edge spectrum similar to that reported for mixed valence perovskites of the same composition with bulklike magnetic properties,[62,63] with a pronounced broad intensity above the edge ascribed to $Mn^{3+/4+}$. But on the other hand, the peak clearly emerging at the low energy side of the L_3-edge for both HR and LR regions can be interpreted as an unexpected presence of divalent Mn.[62,63] Analysis of the O K-edge spectrum changes is not straightforward. Three main features correspond to those observed in case of $La_{1-x}Sr_xMnO_3$ perovskites. The broad peak at 544 eV is attributed to electronic bands of Mn 4sp and La 6sp, while the one at 536 eV is related to a mixture of La 5d with Sr 4d bands; i.e., the spectrum reflects hybridization with the various elements and strongly depends on the oxygen local environment.

Though the above difficulties prevent direct quantification of atomic contents for Mn and O, a close inspection of the right panels of Figure 6 provides evidence of the existence of neat differences in chemical composition for each region. Each panel (g, h, and i) presents the intensity in the three regions of interest (continuous line marked in the PEEM image a), taken at the La, Mn, and O absorption edges (837.8, 641.0, and 529 eV, respectively). In such a way, the increase or decrease of intensity when crossing the HR and LR locations indicates the relative change of the corresponding element after the writing and erasing processes, referred to the respective content in the virgin LSMO, within the same analyzed depth. In contrast to what happens in the case of La and Mn, in which a clear increase of intensity in the HR region is followed by a decrease in the LR region, a decrease of the signal is observed at 529 eV (bottom right panel) in the modified regions.

The above results point to the fact that both electrons and ions play a role on the resistive modifications made on the LSMO films. In fact, the hysteretic behavior of many systems exhibiting resistance switching have been described by mechanisms involving both electronic and ionic transport.[64,65] We note that though other mechanisms involving cation migration as ECM[46] have been proposed, in most MIM junctions, the employed insulating oxides did not contain cations of the active metal or paths for their diffusion. Consequently both an electroforming procedure, before stable resistive switching was observed, and the oxidation and reduction of species during operation were required. Though no electroforming is needed in our case, an unbalanced cation distribution has been found to exist at the LSMO surface. Importantly, the voltage driven change of the ionic species distribution (accumulation or depletion) indicates a modification of the tip−sample interface, but the ultimate implications of this observation, elucidating as well the possible influence on the film microstructure and its relationship with the charge transport mechanism derived from the *IV* characteristic curves need a deeper investigation and will be presented elsewhere.

In summary, we report on a low-energy consumption procedure which permits the reversible electrical resistivity switching in $La_{0.7}Sr_{0.3}MnO_3$ thin films in an extremely local and controlled way. The mechanism by which the LSMO is transformed from its intrinsic metallic to one of nonconducting character is discussed within the frame of electronic and ionic transport within the oxide film. The measured conductance ratios ($I_{ON}/I_{OFF} > 100$) are valuable for high-efficiency amplifiers. An excellent write and erase endurance makes both ON- and OFF-states stable over more than 500 cycles, under continuous readout testing. Moreover, the modifications persist after annealing (tested in the range 5−400 K), show no detectable degradation under magnetic fields (tested up to 3T), and display a long retention time (several months).

A new concept where the writing and erasing processes are made through C-SFM while read out is made through a noninvasive KPM is presented. The dynamic range for the writing process spans a range of $\Delta\Phi \sim 1$ eV and KPM is able to work as a multilevel recording device where an important increase of the integration density (at least by a factor 10) might be achieved. Our capability to fabricate multilevel and switchable resistive nanostructures embedded in low cost oxide thin films can be easily envisaged as a suitable approach toward active electronic elements, in particular for the fabrication of high-density data storage applications.

Acknowledgment. This work has been supported by the Spanish Ministerio de Ciencia e Innovación (Grants. MAT2007-62732, MAT2007-29325-E, MAT2008.01022, and CONSOLIDER CSD2007-00041 NANOSELECT), the EC under Contract No. NMP4-CT-2006-032109 (STREP "SURMOF") and (HIPERCHEM, NESPA), and the Generalitat de Catalunya (Pla de Recerca SGR-0029 and XaRMAE).

Supporting Information Available. Further experimental details in a methods section and four figures illustrating different test performed to illustrate the stability of the reset

© 2010 American Chemical Society

DOI: 10.1021/nl1008162 | *Nano Lett.* **2010,** *10,* 3828--3835

voltage during the endurance tests (S1), to verify the multilevel character of the process (S2), to provide a glance to the storage capabilities of the investigated system (S3), and the durability of the modifications under time, temperature, and magnetic field (S4). This material is available free of charge via the Internet at http://pubs.acs.org.

REFERENCES AND NOTES

(1) Hickmott, T. W. *J. Appl. Phys.* **1962**, *33*, 2669–2682.
(2) Ovshinsky, S. R. *Phys. Rev. Lett.* **1968**, *21*, 1450–1453.
(3) Jo, S. H.; Kim, K. H.; Lu, W. *Nano Lett.* **2009**, *9*, 496–500.
(4) Jo, S. H.; Kim, K. H.; Lu, W. *Nano Lett.* **2009**, *9*, 870–874.
(5) Jo, S. H.; Lu, W. *Nano Lett.* **2008**, *8*, 392–397.
(6) Yang, C. H.; Seidel, J.; Kim, S. Y.; Rossen, P. B.; Yu, P.; Gajek, M.; Chu, Y. H.; Martin, L. W.; Holcomb, M. B.; He, Q.; Maksymovych, P.; Balke, N.; Kalinin, S. V.; Baddorf, A. P.; Basu, S. R.; Scullin, M. L.; Ramesh, R. *Nat. Mater.* **2009**, *8*, 485–493.
(7) Garcia, V.; Fusil, S.; Bouzehouane, K.; Enouz-Vedrenne, S.; Mathur, N. D.; Barthelemy, A.; Bibes, M. *Nature* **2009**, *460*, 81–84.
(8) Wolf, S. A.; Awschalom, D. D.; Buhrman, R. A.; Daughton, J. M.; von Molnar, S.; Roukes, M. L.; Chtchelkanova, A. Y.; Treger, D. M. *Science* **2001**, *294*, 1488–1495.
(9) Gajek, M.; Bibes, M.; Fusil, S.; Bouzehouane, K.; Fontcuberta, J.; Barthelemy, A.; Fert, A. *Nat. Mater.* **2007**, *6*, 296–302.
(10) Meijer, G. I. *Science* **2008**, *319*, 1625–1626.
(11) Sawa, A. *Mater. Today* **2008**, *11*, 28–36.
(12) Beck, A.; Bednorz, J. G.; Gerber, C.; Rossel, C.; Widmer, D. *Appl. Phys. Lett.* **2000**, *77*, 139–141.
(13) Janousch, M.; Meijer, G. I.; Staub, U.; Delley, B.; Karg, S. F.; Andreasson, B. P. *Adv. Mater.* **2007**, *19*, 2232–2235.
(14) Chen, A.; Haddad, S.; Wu, Y. C.; Fang, T. N.; Lan, Z.; Avanzino, S.; Pangrle, S.; Buynoski, M.; Rathor, M.; Cai, W. D.; Tripsas, N.; Bill, C.; VanBuskirk, M.; Taguchi, M. *IEEE Int. Electron Devices Meet., Tech. Dig.* **2005**, *1089*, 765–768.
(15) Chang, S. H.; Lee, J. S.; Chae, S. C.; Lee, S. B.; Liu, C.; Kahng, B.; Kim, D. W.; Noh, T. W. *Phys. Rev. Lett.* **2009**, *102*, No. 026801.
(16) Yang, J. J.; Pickett, M. D.; Li, X. M.; Ohlberg, D. A. A.; Stewart, D. R.; Williams, R. S. *Nat. Nanotechnol.* **2008**, *3*, 429–433.
(17) Choi, B. J.; Jeong, D. S.; Kim, S. K.; Rohde, C.; Choi, S.; Oh, J. H.; Kim, H. J.; Hwang, C. S.; Szot, K.; Waser, R.; Reichenberg, B.; Tiedke, S. *J. Appl. Phys.* **2005**, *98*, No. 033715.
(18) Yang, Y. C.; Pan, F.; Liu, Q.; Liu, M.; Zeng, F. *Nano Lett.* **2009**, *9*, 1636–1643.
(19) Liu, S. Q.; Wu, N. J.; Ignatiev, A. *Appl. Phys. Lett.* **2000**, *76*, 2749–2751.
(20) Asamitsu, A.; Tomioka, Y.; Kuwahara, H.; Tokura, Y. *Nature* **1997**, *388*, 50–52.
(21) Lau, H. K.; Leung, C. W. *J. Appl. Phys.* **2008**, *104*, 123705.
(22) Chen, X.; Wu, N. J.; Strozier, J.; Ignatiev, A. *Appl. Phys. Lett.* **2006**, *89*, No. 063507.
(23) Baikalov, A.; Wang, Y. Q.; Shen, B.; Lorenz, B.; Tsui, S.; Sun, Y. Y.; Xue, Y. Y.; Chu, C. W. *Appl. Phys. Lett.* **2003**, *83*, 957–959.
(24) Waser, R.; Aono, M. *Nat. Mater.* **2007**, *6*, 833–840.
(25) Chudnovskii, F. A.; Odynets, L. L.; Pergament, A. L.; Stefanovich, G. B. *J. Solid State Chem.* **1996**, *122*, 95–99.
(26) Rossel, C.; Meijer, G. I.; Bremaud, D.; Widmer, D. *J. Appl. Phys.* **2001**, *90*, 2892–2898.
(27) Kwon, D.-H.; Kim, K. M.; Jang, J. H.; Jeon, J. M.; Lee, M. H.; Kim, G. H.; Li, X.-S.; Park, G.-S.; Lee, B.; Han, S.; Kim, M.; Hwang, C. S. *Nat. Nanotechnol.* **2010**, *5*, 148–153.
(28) Lee, M.-J.; Han, S.; Jeon, S. H.; Park, B. H.; Kang, B. S.; Ahn, S.-E.; Kim, K. H.; Lee, C. B.; Kim, C. J.; Yoo, I.-K.; Seo, D. H.; Li, X.-S.; Park, J.-B.; Lee, J.-H.; Park, Y. *Nano Lett.* **2009**, *9*, 1476–1481.
(29) Nian, Y. B.; Strozier, J.; Wu, N. J.; Chen, X.; Ignatiev, A. *Phys. Rev. Lett.* **2007**, *98*, 146403.
(30) Rozenberg, M. J.; Inoue, I. H.; Sanchez, M. J. *Phys. Rev. Lett.* **2004**, *92*, 178302.
(31) Inoue, I. H.; Rozenberg, M. J. *Adv. Funct. Mater.* **2008**, *18*, 2289–2292.
(32) Tsui, S.; Baikalov, A.; Cmaidalka, J.; Sun, Y. Y.; Wang, Y. Q.; Yue, Y. Y.; Chu, C. W.; Chen, L.; Jacobson, A. J. *Appl. Phys. Lett.* **2004**, *85*, 317–319.
(33) Odagawa, A.; Kanno, T.; Adachi, H. *J. Appl. Phys.* **2006**, *99*, No. 016101.
(34) Szot, K.; Speier, W.; Bihlmayer, G.; Waser, R. *Nat. Mater.* **2006**, *5*, 312–320.
(35) Muenstermann, R.; Dittmann, R.; Szot, K.; Mi, S. B.; Jia, C. L.; Meuffels, P.; Waser, R. *Appl. Phys. Lett.* **2008**, *93*, No. 023110.
(36) Chen, X.; Wu, N. J.; Strozier, J.; Ignatiev, A. *Appl. Phys. Lett.* **2005**, *87*, 233506.
(37) Shima, H.; Fumiyoshi, T.; Hidenobu, M.; Masashi, Y.; Hiroyuki, A.; Akinori, K. *Phys. Status Solidi RRL* **2008**, *2*, 99–101.
(38) Yoshida, C.; Kinoshita, K.; Yamasaki, T.; Sugiyama, Y. *Appl. Phys. Lett.* **2008**, *93*, No. 042106.
(39) Hasenkox, U.; Mitze, C.; Waser, R.; Arons, R. R.; Pommer, J.; Güntherodt, G. *J. Electroceram.* **1999**, *3*, 255–260.
(40) Moreno, C.; Abellan, P.; Hassini, A.; Ruyter, A.; del Pino, A. P.; Sandiumenge, F.; Casanove, M. J.; Santiso, J.; Puig, T.; Obradors, X. *Adv. Funct. Mater.* **2009**, *19*, 2139–2146.
(41) Hassini, A.; Pomar, A.; Gutierrez, J.; Coll, M.; Roma, N.; Moreno, C.; Ruyter, A.; Puig, T.; Obradors, X. *Supercond. Sci. Technol.* **2007**, *20*, S230–S238.
(42) Gutiérrez, J.; Llordés, A.; Gázquez, J.; Gibert, M.; Romà, N.; Ricart, S.; Pomar, A.; Sandiumenge, F.; T.; Mestres, N.; Puig, T.; Obradors, X. *Nat. Mater.* **2007**, *6*, 367.
(43) Soler-Illia, G. J.; Sanchez, C.; Lebeau, B.; Patarin, J. *Chem. Rev.* **2002**, *102*, 4093–4138.
(44) Schwartz, R. W.; Schneller, T.; Waser, R. *C. R. Chim.* **2004**, *7* (5), 443–461.
(45) Xie, Y. W.; Sun, J. R.; Wang, D. J.; Liang, S.; Shen, B. G. *J. Appl. Phys.* **2006**, *100*, No. 033704.
(46) Waser, R.; Dittmann, R.; Staikov, G.; Szot, K. *Adv. Mater.* **2009**, *21*, 2632–2663.
(47) Blom, P. W. M.; Wolf, R. M.; Cillessen, J. F. M.; Krijn, M. P. C. M. *Phys. Rev. Lett.* **1994**, *73*, 2107.
(48) Harada, T.; Ohkubo, I.; Tsubouchi, K.; Kumigashira, H.; Ohnishi, T.; Lippmaa, M.; Matsumoto, Y.; Koinuma, H.; Oshima, M. *Appl. Phys. Lett.* **2008**, *92*, 222113.
(49) Shang, D. S.; Wang, Q.; Chen, L. D.; Dong, R.; Li, X. M.; Zhang, W. Q. *Phys. Rev. B* **2006**, *73*, 245427.
(50) Xia, Y.; He, W.; Chen, L.; Meng, X.; Liu, Z. *Appl. Phys. Lett.* **2007**, *90*, No. 022907−3.
(51) Sawa, A.; Fujii, T.; Kawasaki, M.; Tokura, Y. *Appl. Phys. Lett.* **2006**, *88*, 232112.
(52) Heike, S.; Watanabe, S.; Wada, Y.; Hashizume, T. *Phys. Rev. Lett.* **1998**, *81*, 890.
(53) Hasegawa, S.; Grey, F. *Surf. Sci.* **2002**, *500*, 84.
(54) Reagor, D. W.; Lee, S. Y.; Li, Y.; Jia, Q. X. *J. Appl. Phys.* **2004**, *95*, 7971–7975.
(55) Nonnenmacher, M.; O'Boyle, M. P.; Wickramasinghe, H. K. *Appl. Phys. Lett.* **1991**, *58*, 2921–2923.
(56) Meister, S.; Schoen, D. T.; Topinka, M. A.; Minor, A. M.; Cui, Y. *Nano Lett.* **2008**, *8*, 4562–4567.
(57) Jung, Y.; Lee, S.-H.; Jennings, A. T.; Agarwal, R. *Nano Lett.* **2008**, *8*, 2056–2062.
(58) Sawa, A.; Yamamoto, A.; Yamada, H.; Fujii, T.; Kawasaki, M.; Matsuno, J.; Tokura, Y. *Appl. Phys. Lett.* **2007**, *90*, 252102.
(59) Bauer, E. *J. Electron Spectrosc. Relat. Phenom.* **2001**, *114−116*, 975–987.
(60) Abbate, M.; de Groot, F. M. F.; Fuggle, J. C.; Fujimori, A.; Strebel, O.; Lopez, F.; Domke, M.; Kaindl, G.; Sawatzky, G. A.; Takano, M.; Takeda, Y.; Eisaki, H.; Uchida, S. *Phys. Rev. B* **1992**, *46*, 4511.
(61) Laan, G. v. d.; Kirkman, I. W. *J. Phys.: Condens. Matter* **1992**, *4*, 4189–4204.
(62) Valencia, S.; Gaupp, A.; Gudat, W.; Abad, L.; Balcells, L.; Cavallaro, A.; Martinez, B.; Palomares, F. J. *Phys. Rev. B* **2006**, *73*, 104402.
(63) Valencia, S.; Gaupp, A.; Gudat, W.; Abad, L.; Balcells, L.; Martinez, B. *Phys. Rev. B* **2007**, *75*, 184431.
(64) Chua, L. O. *IEEE Trans. Circuit Theory* **1971**, *Ct18*, 507–519.
(65) Strukov, D. B.; Snider, G. S.; Stewart, D. R.; Williams, R. S. *Nature* **2008**, *453*, 80–83.

© 2010 American Chemical Society

DOI: 10.1021/nl1008162 | *Nano Lett.* **2010,** *10,* 3828–3835